Paramagnetic ^{14}N MAS NMR without Paramagnetic Shifts: Remarkable Lattice of $LaTiO_2N$ and $CeTiO_2N$ Oxynitride Perovskites

Zili Ma,[†] Richard Dronskowski,[†] Adam Slabon,[‡] and Aleksander Jaworski*[,‡]

[†]*Chair of Solid-State and Quantum Chemistry, Institute of Inorganic Chemistry, RWTH Aachen University, Landoltweg 1, D-52056 Aachen, Germany*

[‡]*Department of Materials and Environmental Chemistry, Stockholm University, SE-106 91 Stockholm, Sweden*

Received September 1, 2020; E-mail: aleksander.jaworski@mmk.su.se

Abstract: ^{14}N magic-angle spinning (MAS) NMR spectra of diamagnetic $LaTiO_2N$ perovskite oxynitride and its paramagnetic counterpart $CeTiO_2N$ are presented. The latter, to the best of our knowledge, constitutes the first high-resolution ^{14}N MAS NMR spectrum collected from paramagnetic solid material. Induced paramagnetic ^{14}N NMR shift due to unpaired $4f$-electrons in $CeTiO_2N$ is non-existent, which is remarkable given the severe paramagnetic effects on surface proton species revealed by ^{1}H NMR, and direct Ce−N contacts in the structure. *Ab initio* molecular orbital calculations predict substantial Ce→^{14}N contact shift interaction under these circumstances, therefore, cannot explain the unprecedented ^{14}N NMR spectrum of $CeTiO_2N$.

$LaTiO_2N$ and other oxynitride semiconductors with perovskite crystal structure exhibit favorable band gaps and visible-light-driven photocatalytic activity for water splitting reactions, hence constitute one of the most promising types of materials for this purpose.[1–10] Local O^{2-}/N^{3-} anion ordering in these systems is predicted to have significant implications on properties such band gaps, and was studied with X-ray, electron, and neutron diffraction, as well as first-principles calculations.[11–18] However, local O^{2-}/N^{3-} ordering occurs on too short length scales to be observed by diffraction techniques.[13] Moreover, O^{2-} and N^{3-} ions differ in charge, ionic radii, and coordination preferences, thus are not expected to occupy the same positions, as it is enforced in structures derived from diffraction measurements, which are biased by averaging. On the other hand, solid-state NMR probes nitrogen atoms directly, regardless of chemical/structural disorder. Therefore, in this work we present ^{14}N MAS NMR spectra of $LaTiO_2N$ and its paramagnetic counterpart $CeTiO_2N$. Assessment on how these spectra compare, given the paramagnetic NMR interactions arising in the latter, may provide further insights into Ce/N/O arrangements in these structures. The paramagnetic nature of $CeTiO_2N$ was revealed by magnetic measurements resulting in Weiss constant $\theta = -28$ K and effective magnetic moment $\mu_{\text{eff}} = 2.43$,[13] in line with that expected for free Ce^{3+} ion (2.54), in contrast to potential occurrence of Ti^{3+} (1.73). To the best of our knowledge, this is the first reported high-resolution ^{14}N MAS NMR spectrum of solid paramagnetic material, considering that previous attempts were performed under static conditions and cryogenic temperatures.[19–21]

Despite 99.6% natural abundance of ^{14}N isotope, solid-state ^{14}N NMR studies of materials are very rare. This is due to the spin $I = 1$ and considerable nuclear quadrupole moment of ^{14}N, which result in signals that are severely broadened by quadrupolar interaction, imposing serious challenges with respect to signal excitation, processing, and interpretation. However, as revealed by recent studies on Ta- and Nb-based oxynitrides, and N-doped $BaTiO_3$, ^{14}N NMR signals of these materials are unusually narrow, implying that quadrupolar interaction vanishes due to the high local symmetry of N^{3-} moieties.[8,10,22,23] This offers the unique opportunity to get insight into ^{14}N paramagnetic interactions in the solid-state, which has not been investigated with MAS NMR before.

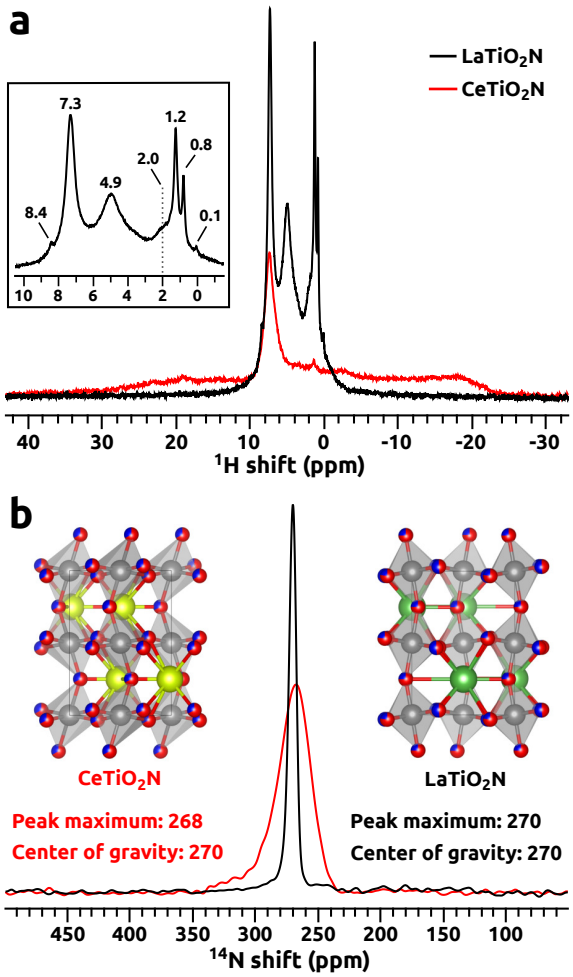

Figure 1. ^{1}H (a) and ^{14}N (b) MAS NMR spectra of $LaTiO_2N$ (black traces) and $CeTiO_2N$ (red traces) collected at 14.1 T and 60 kHz MAS rate. Inset in panel a shows zoomed ^{1}H NMR signals from $LaTiO_2N$. Insets in panel b display crystal unit cells of both materials with Ce atoms as yellow, La as green, Ti grey, and O/N red/blue. Crystallographic data from refs.[13,14]

For paramagnetic systems the NMR shift can be expressed as:

$$\delta = \delta_{orb} + \delta_{con} + \delta_{pc} \quad (1)$$

where δ_{orb} term corresponds to orbital "chemical" shift, the sole shift contribution in diamagnetic systems, whereas the latter two terms arise due to the presence of unpaired electrons. δ_{con} is associated with elecron-nucleus hyperfine coupling constant (HFCC) and denotes the effect of through-bond polarization called "contact shift", which is operative in close vicinity to paramagnetic ion. δ_{pc} term called "pseudocontact shift" (PCS) originate from electron-nucleus dipolar coupling and magnetic anisotropy of paramagnetic center, and is long-range in nature ($1/r^3$). Paramagnetic lanthanide (Ln) ions can induce PCS effects for NMR-active nuclei at the distances as long as 25−40 Å.[24] This is exploited in biomolecular NMR, where paramagnetic ions are used as "shift tags" for structure elucidation of large molecular systems.[25–27] On the other hand, solid-state NMR studies of materials incorporating paramagnetic lanthanide ions are scarce. At short distances between the nuclei of NMR interest and paramagnetic Ln^{3+} ions in solids, both contact and pseudocontact mechanisms contribute to the NMR shift, which complicates data interpretation. ^{89}Y MAS NMR studies of Ln-substituted yttrium pyrochlores $Y_{2-x}Ln_xSn_2O_7$ and $Y_{2-x}Ln_xTi_2O_7$ revealed significant induced paramagnetic shifts of ^{89}Y NMR signals from yttrium sites in close proximities to paramagnetic Ln^{3+} ions, compared to the signals from diamagnetic $Y_2Sn_2O_7$ and $Y_2Ti_2O_7$.[28] Similar effects were observed for ^{27}Al resonances upon incorporation of Ce (or other paramagnetic lanthanides) in $Y_3Al_5O_{12}$ (YAG),[29–31] as well as for ^{43}Ca and ^{45}Sc NMR signals from $CaSc_2O_4$ doped with Ce.[32] However, the assessment on δ_{con}/δ_{pc} mechanisms could not be established. Note that in aforementioned materials contacts between the probed nuclei and paramagnetic Ln^{3+} ions are not direct but via oxygen bridges (Ln−O−X), with distances $r_{Ln-X} \gtrsim 3$ Å. ^{17}O MAS NMR studies of paramagnetic lanthanide oxides Ln_2O_3 (probed atoms are directly bonded to paramagnetic Ln^{3+} ions) revealed substantial ^{17}O shifts (hundreds to thousands ppm), with contributions from all three terms: δ_{orb}, δ_{con}, and δ_{pc}.[33,34] In this work we explore corresponding effects for nitrogen with ^{14}N MAS NMR on $LaTiO_2N$ and $CeTiO_2N$ oxynitride perovskites.

Let us first consider the ^{1}H MAS NMR spectrum of $LaTiO_2N$ photocatalyst surface, which is presented in Figure 1(a), black trace. Proton signal at 4.9 ppm corresponds to physisorbed H_2O, whereas remaining resonances originate from different types of bridging ($>OH_B$) and terminal hydroxyl groups ($-OH_T$).[35] In contrast, surface proton signals from paramagnetic $CeTiO_2N$ (Figure 1(a), red trace) are strongly affected by the presence of unpaired electrons from Ce^{3+} ions. Spectrum is severely broadened as a result of both paramagnetic NMR shift interactions and relaxation enhancement.[27] Only signal at 7.3 ppm is moderately affected, which indicates that it originates from protons being the most distant ones from Ce^{3+} ions.

The ^{14}N MAS NMR spectrum of $LaTiO_2N$ is shown in Figure 1(b), black trace. Narrow signal at 270 ppm is consistent with data reported for other diamagnetic oxynitride perovskites, and are collected in Table 1. Although these oxynitrides develope space groups with lower than cubic symmetry as a result of octahedra tilts and rotations upon substitutions of different cations, ^{14}N NMR shifts are basically unchanged, indicating that local environments of nitrogen are almost identical.

Table 1. ^{14}N NMR shifts in oxynitride perovskites

Formula	Space group	^{14}N shift (ppm)
$CaNbO_2N$	$Pnma$[36]	270[8]
$SrNbO_2N$	$I4/mcm$[36]	271[8]
$BaNbO_2N$	$Pm\bar{3}m$[36]	270[8]
$LaNbON_2$	$Pnma$[37]	271[8]
$CaTaO_2N$	$Pnma$[36]	270−271[8,10,23]
$SrTaO_2N$	$I4/mcm$[36]	271−272[8,23]
$BaTaO_2N$	$Pm\bar{3}m$[36]	269−270[8,23]
$BaTi(O,N)_3$	$P4mm$[38]	271[22]
$LaTaON_2$	$Imma$[16]	270[8]
$LaTiO_2N$	$Imma$[14]	270 (this work)
$CeTiO_2N$	$Pnma$[13]	268 (this work)

The ^{14}N MAS NMR spectrum of paramagnetic $CeTiO_2N$ is presented in Figure 1(b), red trace. Despite being broader and a little bit less symmetric, ^{14}N signal from $CeTiO_2N$ exhibits no induced paramagnetic shift due to unpaired $4f$ electrons when compared to its $LaTiO_2N$ counterpart and other diamagnetic oxynitride perovskites in Table 1. This is remarkable given the direct Ce−N contacts in the network and strong paramagnetic effects on surface protons [Fig. 1(a)]. This counterintuitive result could be explained by the cancellation of orbital and paramagnetic shift contributions with opposite signs, as it is partially the case for ^{17}O NMR shifts in Sm_2O_3.[34] However, based on the ^{14}N NMR data in Table 1 for ten diamagnetic oxynitride perovskites incorporating variety of metal ions, it is safe to assume that δ_{orb} does not change for $CeTiO_2N$ as well, so induced paramagnetic shift has to be zero, or at least δ_{con} and δ_{pc} have to cancel each other out.

To explore these scenarios, induced paramagnetic ^{14}N NMR shifts were evaluated in terms of electron paramagnetic resonance (EPR) parameters by applying the formalism of Moon and Patchkovskii,[39] and Vaara[40–43] to hypothetical cluster model derived from $CeTiO_2N$ crystal lattice. The calculations of ^{14}N hyperfine coupling tensors and electronic g-tensor of Ce were performed with *ab initio* quantum chemistry methods: domain-based local pair natural orbital coupled-cluster singlets and doublets (DLPNO-CCSD)[44] and multireference perturbation theory (CASSCF/NEVPT2),[45] respectively (see Supporting Information for details). Although this theoretical approach employed crude approximation of (averaged) structure derived from diffraction measurements and no Madelung field, nonetheless the molecular orbital theory is helpful because it provides upper/lower bounds of the range of ^{14}N HFCCs expected at the Ce−N distances representative for the $CeTiO_2N$ crystal lattice, and insight into relative magnitudes of contact and PCS effects as well.

Predicted ^{14}N HFCCs for nitrogen positions at the distances of 2.1 and 2.5 Å from Ce in the $CeTiO_2N$ model are −2.0 and −0.9 MHz, respectively (Table S4). These values are in the same range as the experimental estimates of −2.2 and −0.6 MHz for ^{17}O HFCCs in cubic Eu_2O_3 and Sm_2O_3 (Ln−O distances of 2.3−2.4 Å),[34] and the older experimental value of −2.7 MHz estimated for ^{17}O HFCC in the series of paramagnetic lanthanide oxides (Ln_2O_3).[33] Both ^{14}N and ^{17}O HFCCs are negative due to polarization mechanism mediated by lanthanide $6s$ orbitals ($4f$ orbitals do not participate in chemical bonding to any greater extent).[34] For nitrogen positions at the distances $\geqslant$3.3 Å from Ce, pre-

dicted magnitudes of ^{14}N HFCCs are <0.05 MHz. However, the scenario that nitrogen atoms experience only distances ⩾3.3 Å from Ce is unrealistic, considering the $CeTiO_2N$ crystal structure.

Calculated induced ^{14}N paramagnetic contact shifts for nitrogen atoms at the distances of 2.1 and 2.5 Å from Ce^{3+} ions are −498 and −213 ppm, respectively (Table S7), whereas magnitudes of pseudocontact shifts are <30 ppm and diminish to <10 ppm already at the distances ⩾3.3 Å. Therefore, long-range effects from distant paramagnetic centers are unlikely to counteract substantial contact shifts of close Ce−N contacts, given that next nearest Ce neighbors are >4.5 Å away.

Hence, we conclude that averaged crystal structure obtained by diffraction techniques does not provide basis for understanding of experimental ^{14}N MAS NMR spectrum of $CeTiO_2N$, and more work is needed to gain insight into local structures in these materials. Consequently, the lack of paramagnetic shift in the ^{14}N MAS NMR spectrum of $CeTiO_2N$ we attribute to unique symmetry and Ce−O/N arrangement in the $CeTiO_2N$ lattice that leads to remarkable cancellation effects for interactions with distinct physical origins and different spatial dependencies.

METHODS

For synthesis of $LaTiO_2N$, the $La_2Ti_2O_7$ precursor oxide was synthesized by a conventional solid-state reaction with KCl as flux, similarly to our previous work.[10] In short, starting materials of 1.5 mmol La_2O_3 (99.9 wt %, Fluka), 3 mmol TiO_2 (99.3 wt %, VWR Chemicals) and 15 mmol KCl (99.5 wt %, Grüssing) were adequately ground. Mixture was placed in an alumina crucible to be heated to 1423 K for 8 h at a ramping rate of 10 K/min under ambient atmosphere and then cooled to room temperature at a rate of 10 K/min.[3] The product was ground and washed with distilled water to completely remove the flux agent. A typical thermal ammonalysis process was employed to convert $La_2Ti_2O_7$ into $LaTiO_2N$. Briefly, 100 mg of $La_2Ti_2O_7$ was placed into an alumina crucible in a tube furnace and was subsequently heated under a constant flow of NH_3 (15 mL/min) and H_2 (5 mL/min) at 1223 K for 15 h at a ramping rate of 10 K/min. After cooling down to room temperature, the final $LaTiO_2N$ product can be obtained.

Quaternary oxynitrides can also be prepared via one step NH_3-assisted flux-mediated route.[46,47] Cerium can exist with oxidation state of Ce^{4+}, i.e. CeO_2. Thus, one step NH_3-assisted flux-mediated route was used to synthesize CeTiO2N by *in situ* reducing Ce^{4+} to Ce^{3+}. Typically, starting materials of 1 mmol CeO2 (99.9 wt %, ABCR Chemicals) and 1 mmol TiO2 (99.3 99.9 wt %, VWR Chemicals) were mixed with 9 mmol LiCl (99 99.9 wt %, Alfa Aesar) by pestle. The mixture placed into an alumina crucible in a tube furnace and was subsequently heated under a constant flow of NH_3 (15 mL/min) and H_2 (5 mL/min) at 1223 K for 15 h at a ramping rate of 10 K/min. After cooling down to room temperature, the product was washed with distilled water to obtain $CeTiO_2N$ by removing the flux agent.

X-ray powder diffraction (XRD) patterns of synthesized $LaTiO_2N$ and $CeTiO_2N$ were recorded in the transmission mode on a STOE STADI-P diffractometer (Cu Kα_1 radiation) equipped with a DECTRIS Mythen 1K detector. See Figure 2.

Solid-state ^{1}H and ^{14}N MAS NMR spectra were acquired at a magnetic field strength of 14.1 T (Larmor frequencies of 600.1 and 43.4 MHz, respectively) with a Bruker Avance III spectrometer equipped with a 1.3 mm MAS probehead and employing MAS rate of 60.00 kHz. ^{1}H NMR acquisitions were performed with rotor-synchronized, double-adiabatic spin-echo sequence with a 90 degree excitation pulse of 1.1 μs, followed by two 50.0 μs tanh/tan short high-power adiabatic pulses[48,49] with 5 MHz frequency sweep.[50] All pulses operated at a nutation frequency of 210 kHz. 256 signal transients with 5 s relaxation delay were accumulated. ^{14}N MAS NMR spectra were collected using single pulse "Bloch-decay" protocol with 3.0 μs 90 degree excitation pulse and 65536 scans collected with 1 s relaxation delay. ^{1}H shifts were referenced using neat tetramethylsilane (TMS) at 0 ppm, whereas ^{14}N shifts to solid NH_4Cl at 0 ppm (−342.4 ppm with respect to nitromethane).

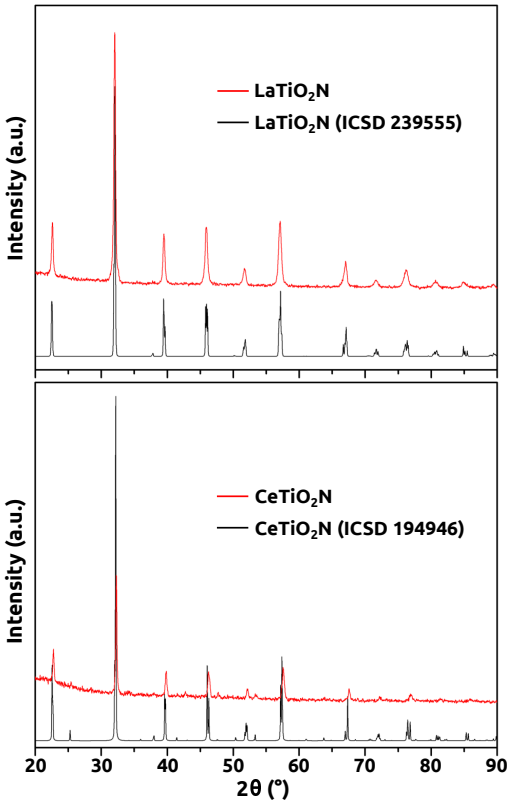

Figure 2. X-ray powder diffraction patterns of synthesized $LaTiO_2N$ and $CeTiO_2N$ samples shown with reference data.[13,14]

Acknowledgement Z.M. would like to thank the China Scholarship Council for a PhD scholarship. A.J. acknowledges very useful discussions with Professor Juha Vaara regarding computations of EPR parameters, and with Professor Andrew J. Pell on paramagnetic NMR.

Supporting Information Available: Theoretical methods. This material is available free of charge via the Internet at `http://pubs.acs.org/`.

References

(1) Kudo, A.; Miseki, Y. Heterogeneous Photocatalyst Materials for Water Splitting. *Chem. Soc. Rev.* **2009**, *38*, 253–278.
(2) Yerga, R. M. N.; Galván, M. C. A.; del Valle, F.; de la Mano, J. A. V.; Fierro, J. L. G. Water Splitting on Semiconductor Catalysts under Visible-Light Irradiation. *ChemSusChem* **2009**, *2*, 471–485.
(3) Zhang, F.; Yamakata, A.; Maeda, K.; Moriya, Y.; Takata, T.; Kubota, J.; Teshima, K.; Oishi, S.; Domen, K. Cobalt-Modified Porous Single-Crystalline $LaTiO_2N$ for Highly Efficient Water

Oxidation under Visible Light. *J. Am. Chem. Soc.* **2012**, *134*, 8348–8351.
(4) Tong, H.; Ouyang, S.; Bi, Y.; Umezawa, N.; Oshikiri, M.; Ye, J. Nano-photocatalytic Materials: Possibilities and Challenges. *Adv. Mater.* **2012**, *24*, 229–251.
(5) Hisatomi, T.; Katayama, C.; Moriya, Y.; Minegishi, T.; Katayama, M.; Nishiyama, H.; Yamada, T.; Domen, K. Photocatalytic Oxygen Evolution Using $BaNbO_2N$ Modified with cobalt oxide under photoexcitation up to 740 nm. *Energy Environ. Sci.* **2013**, *6*, 3595–3599.
(6) Matsukawa, M.; Ishikawa, R.; Hisatomi, T.; Moriya, Y.; Shibata, N.; Kubota, J.; Ikuhara, Y.; Domen, K. Enhancing Photocatalytic Activity of $LaTiO_2N$ by Removal of Surface Reconstruction Layer. *Nano Lett.* **2014**, *14*, 1038–1041.
(7) Akiyama, S.; Nakabayashi, M.; Shibata, N.; Minegishi, T.; Asakura, Y.; Abdulla-Al-Mamun, M.; Hisatomi, T.; Nishiyama, H.; Katayama, M.; Yamada, T.; Domen, K. Highly Efficient Water Oxidation Photoanode Made of Surface Modified $LaTiO_2N$ Particles. *Small* **2016**, *12*, 5468–5476.
(8) Cordes, N.; Bräuniger, T.; Schnick, W. Ammonothermal Synthesis of $EAMO_2N$ (EA=Sr, Ba; M=Nb, Ta) Perovskites and ^{14}N Solid-State NMR Spectroscopic Investigations of $AM(O,N)_3$ (A=Ca, Ba, La). *Eur. J. Inorg. Chem.* **2018**, 5019–5026.
(9) Ma, Z.; Thersleff, T.; Görne, A.; Cordes, N.; Liu, J. S., Y; Rokicińska, A.; Schichtl, Z. G.; Coridan, R. H.; Kuśtrowski, P.; Schnick, W.; Dronskowski, R.; Slabon, A. Quaternary Core-Shell Oxynitride Nanowire Photoanode Containing a Hole-Extraction Gradient for Photoelectrochemical Water Oxidation. *ACS Appl. Mater. Interfaces* **2019**, *11*, 19077–19086.
(10) Ma, Z.; Jaworski, A.; George, J.; Rokicińska, A.; Thersleff, T.; Budnyak, T. M.; Hautier, G.; Pell, A. J.; Dronskowski, R.; Kuśtrowski, P.; Slabon, A. Exploring the Origins of Improved Photocurrent by Acidic Treatment for Quaternary Tantalum-Based Oxynitride Photoanodes on the Example of $CaTaO_2N$. *J. Phys. Chem. C* **2020**, *124*, 152–160.
(11) Fuertes, A. Synthesis and Properties of Functional Oxynitrides−from Photocatalysts to CMR Materials. *Dalton Trans.* **2010**, *39*, 5942–5948.
(12) Yang, M.; Oró-Solé, J.; Rodgers, J. A.; Jorge, A. B.; Fuertes, A.; Attfield, J. P. Synthesis and Properties of Functional Oxynitrides−from Photocatalysts to CMR Materials. *Nature Chemistry* **2011**, *3*, 47–52.
(13) Porter, S. H.; Huang, Z.; Cheng, Z.; Avdeev, M.; Chen, Z.; Dou, S.; Woodward, P. M. Structural and Magnetic Properties of $R\mathrm{TiNO}_2$ (R=Ce, Pr, Nd) Perovskite Nitride Oxides. *J. Solid State Chem.* **2015**, *226*, 279–285.
(14) Habu, D.; Masubuchi, Y.; Torii, S.; Kamiyama, T.; Kikkawa, S. Crystal Structure Study of Dielectric Oxynitride Perovskites of $La_{1-x}Sr_xTiO_{2+x}N_{1-x}$. *J. Solid State Chem.* **2016**, *237*, 254–257.
(15) Wolff, H.; Dronskowski, R. First-Principles and Molecular-Dynamics Study of Structure and Bonding in Perovskite-Type Oxynitrides ABO_2N (A=Ca, Sr, Ba; B=Ta, Nb). *J. Comput. Chem.* **2008**, *29*, 2260–2267.
(16) Porter, S. H.; Huang, Z.; Woodward, P. M. Study of Anion Order/Disorder in $RTaN_2O$ (R=La, Ce, Pr) Perovskite Nitride Oxides. *Cryst.Growth Des.* **2014**, *14*, 117–125.
(17) Kubo, A.; Giorgi, G.; Yamashita, K. Anion Ordering in $CaTaO_2N$: Structural Impact on the Photocatalytic Activity. Insights from First-Principles. *Chem. Mater.* **2017**, *29*, 539–545.
(18) Xu, X.; Jiang, H. Anion Order in Perovskite Oxynitrides AMO_2N (A=Ba, Sr, Ca; M=Ta, Nb): A First-Principles Based Investigation. *RSC Adv.* **2020**, *10*, 24410–24418.
(19) Shulman, R. G.; Wyluda, B. J. Nuclear Magnetic Resonance Shifts in Rare Earth Nitrides. *J. Phys. Chem. Solids* **1962**, *23*, 166.
(20) Magnum, B. W.; Utton, D. B. NMR of ^{14}N in Cerous Magnesium Nitrate Hydrate. *Physica* **1972**, *60*, 63–72.
(21) Takao, K.; Liu, Z.; Uji, K.; Waki, T.; Tabata, Y.; Watanabe, I.; Nakamura, H. Paramagnetic-to-Nonmagnetic Transition in Antiperovskite Nitride Cr_3GeN Studied by ^{14}N NMR and μSR. *J. Phys.: Conf. Ser.* **2017**, *868*, 012021.
(22) Bräuniger, T.; Müller, T.; Pampel, A.; Abicht, H. P. Study of Oxygen-Nitrogen Replacement in $BaTiO_3$ by ^{14}N Solid-State Nuclear Magnetic Resonance. *Chem Mater.* **2005**, *17*, 4114–4117.
(23) Kim, Y.; Paik, Y. Bond Covalency in Perovskite Oxynitrides $A\mathrm{TaO}_2\mathrm{N}$ (A=Ca, Sr, Ba) Studied by ^{14}N NMR Spectroscopy. *Solid State Sciences* **2012**, *14*, 580–582.
(24) Allegrozzi, M.; Bertini, I.; Janik, M. B. L.; Lee, Y. M.; Liu, G.; Luchinat, C. Lanthanide-Induced Pseudocontact Shifts for Solution Structure Refinements of Macromolecules in Shells up to 40 Å from the Metal Ion. *J. Am. Chem. Soc.* **2000**, *122*, 4154–4161.
(25) Bertini, I.; Luchinat, C.; Parigi, G. Paramagnetic Constraints: An Aid for Quick Solution Structure Determination of Paramagnetic Metalloproteins. *Concepts Magn. Reson.* **2002**, *14*, 259–286.
(26) Benda, L.; Mareš, J.; Ravera, E.; Parigi, G.; Luchinat, C.; Kaupp, M.; Vaara, J. Pseudo-Contact NMR Shifts over the Paramagnetic Metalloprotein CoMMP-12 from First Principles. *Angew. Chem.* **2016**, *128*, 14933–14937.
(27) Pell, A. J.; Pintacuda, G.; Grey, C. Paramagnetic NMR in Solution and the Solid State. *Prog. Nucl. Mag. Res. Sp.* **2019**, *111*, 1–271.
(28) Grey, C. P.; Smith, M. E.; Cheetham, A. K.; Dobson, C. M.; Dupree, R. ^{89}Y MAS NMR Study of Rare-Earth Pyrochlores: Paramagnetic Shifts in the Solid State. *J. Am. Chem. Soc.* **1990**, *112*, 4670–4675.
(29) George, N. C.; Pell, A. J.; Dantelle, G.; Page, K.; Llobet, A.; Balasubramanian, M.; Pintacuda, G.; Chmelka, B. F.; Seshadri, R. Local Environments of Dilute Activator Ions in the Solid-State Lighting Phosphor $Y_{3-x}Al_5O_{12}$. *Chem. Mater.* **2013**, *25*, 3979–3995.
(30) McCarty, R. J.; Stebbins, J. F. Investigating Lanthanide Dopant Distributions in Yttrium Aluminum Garnet (YAG) Using Solid State Paramagnetic NMR. *Solid State Nucl. Magn. Reson.* **2016**, *79*, 11–22.
(31) Carvalho, J. P.; Jaworski, A.; Brady, M. J.; Pell, A. J. Separation of Quadrupolar and Paramagnetic Shift Interactions with TOP-STMAS/MQMAS in Solid-State Lighting Phosphors. *Magn. Reson. Chem.* **2020**, 1–16.
(32) George, N. C.; Brgoch, J.; Pell, A. J.; Cozzan, C.; Jaffe, A.; Dantelle, G.; Llobet, A.; Pintacuda, G.; Seshadri, R.; Chmelka, B. F. Correlating Local Compositions and Structures with the MacroscopicOptical Properties of Ce^{3+}-Doped $CaSc_2O_4$, an Efficient Green-Emitting Phosphor. *Chem. Mater.* **2017**, *29*, 3538–3546.
(33) Yang, S.; Shore, J.; Oldfield, E. Oxygen-17 Nuclear Magnetic Resonance Spectroscopic Study of the Lanthanide Oxides. *J. Magn. Reson.* **1992**, *99*, 408–412.
(34) Hope, M. A.; Halat, D. M.; Grey, C. P. A ^{17}O Paramagnetic NMR Study of Sm_2O_3, Eu_2O_3, and Sm/Eu-substituted CeO_2. *Solid State Nucl. Magn. Reson.* **2019**, *102*, 21–30.
(35) Chen, J. et al. Interactions of Oxide Surfaces with Water Revealed with Solid-State NMR Spectroscopy. *J. Am. Chem. Soc.* **2020**, *142*, 11173–11182.
(36) Kim, Y. I.; Woodward, P. M.; Baba-Kishi, K. Z.; Tai, C. W. Characterization of the Structural, Optical, and Dielectric Properties of Oxynitride Perovskites AMO_2N (A=Ba, Sr, Ca; M=Ta, Nb). *Chem. Mater.* **2004**, *16*, 1267–1276.
(37) Logvinovich, D.; Ebbinghaus, S. G.; Reller, A.; Marozau, I.; Ferri, D.; Weidenkaff, A. Synthesis, Crystal Structure and Optical Properties of $LaNbON_2$. *Z. Anorg. Allg. Chem.* **2010**, *636*, 905–912.
(38) Buttner, R. H.; Maslen, E. N. Structural Parameters and Electron Difference Density in $BaTiO_3$. *Acta Cryst.* **1992**, *48*, 764–769.
(39) Moon, S.; Patchkovskii, S.; in, *Calculation of NMR and EPR Parameters: Theory and Applications*; Wiley-VCH: Weinheim, 2004.
(40) Pennanen, T. O.; Vaara, J. Density-Functional Calculations of Relativistic Spin-Orbit Effects on Nuclear Magnetic Shielding in Paramagnetic Molecules. *J. Chem. Phys.* **2005**, *123*, 174102.
(41) Pennanen, T. O.; Vaara, J. Nuclear Magnetic Resonance Chemical Shift in an Arbitrary Electronic Spin State. *Phys. Rev. Lett.* **2008**, *100*, 133002.
(42) Rouf, S. A.; Mareš, J.; Vaara, J. ^1H Chemical Shifts in Paramagnetic Co(II) Pyrazolylborate Complexes: A First-Principles Study. *J. Chem. Theory Comput.* **2015**, *11*, 1683–1691.
(43) Vaara, J.; Rouf, S. A.; Mareš, J. Magnetic Couplings in the Chemical Shift of Paramagnetic NMR. *J. Chem. Theory Comput.* **2015**, *11*, 4840–4849.
(44) Saitow, M.; Neese, F. Accurate Spin-Densities Based on the Domain-Based Local Pair-Natural Orbital Coupled-Cluster Theory. *J. Chem. Phys.* **2018**, *149*, 034104.
(45) Ganyushin, D.; Neese, F. A Fully Variational Spin-Orbit Coupled Complete Active Space Self-Consistent Field Approach: Application to Electron Paramagnetic Resonance g-Tensors. *J. Chem. Phys.* **2013**, *138*, 104113.
(46) Zhang, L.; Song, Y.; Feng, J.; Fang, T.; Zhong, Y.; Zhaosheng, L.; Zou, Z. Photoelectrochemical Water Oxidation of $LaTaON_2$ under Visible-Light Irradiation. *Int. J. Hydrogen Energy* **2014**, *39*, 7697–7704.
(47) Kawashima, K.; Hojamberdiev, M.; Wagata, H.; Yubuta, K.; Vequizo, J. J. M.; Yamakata, A.; Oishi, S.; Domen, K.; Teshima, K. NH_3-Assisted Flux-Mediated Direct Growth of $LaTiO_2N$ Crystallites for Visible-Light-Induced Water Splitting. *J. Phys. Chem. C* **2015**, *119*, 15896–15904.
(48) Hwang, T. L.; van Zijl, P. C. M.; Garwood, M. Fast Broadband Inversion by Adiabatic Pulses. *J. Mag. Reson.* **1998**, *133*, 200–203.
(49) Kervern, G.; Pintacuda, G.; Emsley, L. Fast Adiabatic Pulses for Solid-State NMR of Paramagnetic Systems. *Chem. Phys. Lett.* **2007**, *435*, 157–162.
(50) Pell, A. J.; Pintacuda, G. Broadband Solid-State MAS NMR of Paramagnetic Systems. *Prog. Nucl. Magn. Reson. Spectrosc.* **2015**, *84-85*, 33–72.